Ingeniería Energética
ISSN: 1815-5901
Instituto Superior Politécnico José A. Echeverría.Cujae

Namoune, Abdelhadi; Taleb, Rachid; Benzidane, Mohammed Ridha
Diseño y simulación de inductor cuadrado integrado
en convertidor elevador para aplicaciones fotovoltaicas
Ingeniería Energética, vol. XLIV, núm. 1, 2023, Enero-Abril, pp. 1-12
Instituto Superior Politécnico José A. Echeverría.Cujae

Ingeniería Energética,
2023, 44(1): e0501,enero-abril,
ISSN 1815-5901

Universidad Tecnológica de La Habana
José Antonio Echeverría

Artículo original

Design and simulation of integrated spiral inductor a boost converter for photovoltaic application

Diseño y simulación de inductor cuadrado integrado en convertidor elevador para aplicaciones fotovoltaicas

Abdelhadi Namoune[I,*], Rachid Taleb[II], Mohammed Ridha Benzidane[III]

[I]Relizane University, Relizane, Algeria
[II]Hassiba Benbouali University of Chlef, Chlef, Algeria
[III]Abdelhamid Ibn Badis University, Mostaganem, Algeria
[*]Autor de correspondencia: abdelhadi.namoune@cu-relizane.dz or namoune.abdelhadi@gmail.com

Received: 4 de noviembre de 2022 Approved: 5 de enero de 2023

RESUMEN/ *ABSTRACT*
The microelectronics industry is in a constant race for high-efficiency integrated electronic components for photovoltaic applications. This paper presents a method of dimensioning a spiral inductor integrated in boost converter application a photovoltaic. We are interested in designing and dimensioning a spiral inductor integrated into a Boost converter in this work. The incorporation of passive energy components allows reducing the size of these structures to a minimum space requirement while ensuring acceptable efficiency and improving the characteristics of energy conversion systems as well as reducing their cost. The chosen compact model's electrical, magnetic and frequency behavior, containing all the integrated inductor technological parameters, is described by analytical expressions whose resolution is made using simulation COMSOL software. To validate the geometric dimensions and technological parameters, We have simulated the system of the solar booster converter containing the electrical circuit of the spiral inductor by software PSIM.
Key words: Integration, Boost converter, Spiral inductor, Photovoltaic, passive power.

La industria de la microelectrónica está en una carrera constante por componentes electrónicos integrados de alta eficiencia para aplicaciones fotovoltaicas. Este artículo presenta un método para dimensionar un inductor en espiral integrado en una aplicación de convertidor elevador fotovoltaico. Estamos interesados en diseñar y dimensionar un inductor en espiral integrado en un convertidor Boost en este trabajo. La incorporación de componentes energéticos pasivos permite reducir el tamaño de estas estructuras a un mínimo requerimiento de espacio asegurando una eficiencia aceptable y mejorando las características de los sistemas de conversión de energía así como reduciendo su coste. El modelo compacto elegido eléctrico, comportamiento magnético y de frecuencia, que contiene todos los parámetros tecnológicos del inductor integrado, se describe mediante expresiones analíticas cuya resolución se realiza mediante el software de simulación COMSOL. Validar las dimensiones geométricas y los parámetros tecnológicos, Hemos simulado el sistema del convertidor solar booster que contiene el circuito eléctrico del inductor espiral mediante el software PSIM.
Palabras clave: *Integración, Convertidor de impulsar, inductor espiral, Fotovoltaica, poder pasivo.*

INTRODUCTION

Recent developments in photovoltaic field topologies show an increasingly important insertion of power electronics. The PV topologies with central inverters fail regarding their performance and maintaining process compared to topologies with power optimizers or micro-inverters [1, 2]. Even resorting to modular topologies with micro-inverters or power-optimizers, is not expected because of their high cost, especially for large-scale systems [3, 4]. Therefore, the integration of the passive components of these converters becomes an inevitable solution in order to solve the cost and profile problems.

How to cite this article:
Abdelhadi Namoune, Rachid Taleb and Mohammed Ridha Benzidane. Design and simulation of integrated spiral inductor a boost converter for photovoltaic application. Ingeniería Energética. 2023. 44(1), enero/abril. ISSN: 1815-5901.

The tendency in power converters toward high power density, high operating frequency, and low profile has revealed many constraints in the use of standard wire-wound . Planar inductors practically remove some inconveniences of traditional wire-wound kinds. As a result, planar has grown in popularity in high-frequency power converters at recent years [5, 6]. The work presented in this paper deals with the miniaturization of a Boost DC/DC converter dedicated for photovoltaic applications, as well as the improvement of its performances. Our main objective is to design DC-DC converter of very small size which can be inserted at the back of the PV module.

METHODOLOGY AND MODELLING

The boost converter (figure 1), is a type of DC-DC converter that can provide an output voltage greater than the input voltage [7]. Due to the conservation of energy, the input power of the boost converter must be equal to the output, which means that the current at the boost's output is less than the input current. This sort of converter is frequently utilized in PV applications due to its high efficiency and ease of implementation [8].

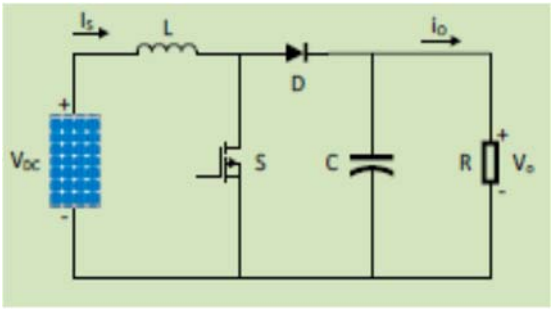

Fig. 1. Conventional Boost Converter [8]

Since the aim of this study is to reduce the size and maintain the performance, a small solar panel containing polycrystalline coated solar cells protected by a solid outer frame was used, which has the characteristics mentioned in table 1.

Table 1. Characteristics of the used solar panel [9]

Solar module	Value
Maximum working voltage	3,3 [V]
Maximum current	0,15 [A]
Maximum power *Pmax*	0,45 [W]
Min working voltage	3 [V]
Maximum power tolerance	15%
Working temperature	-45°C to +85 °C

a) Design of DC DC converter

As shown in the figure 2, a Boost converter including a PV voltage source, an inductor L, a switch, a capacitor C and a load resistor R. In practice a MOSFET and Diode are used instead of switches. The switch of the boost converter is controlled with a PWM signal. Two operational modes arise from turning the switch “ON” and “OFF” with the PWM signal. The explanation of the boost converter and PWM is offered in detail in [10].

The input and output voltage relationship is controlled by the switch duty cycle, D, according to the following equation (1), [11]:

$$V_{out} = \frac{V_{in}}{1 - D} \tag{1}$$

Where, Vin is the input voltage, Vout is the output voltage, and D is the Duty cycle

To operate the boost converter in this study we chose the continuous connection mode (CCM), hence the current in the inductor (I_L) never drops to zero, as shown in equation (2).

$$I_L = I_{max} = \frac{V_{in}}{V_{out}}.(\alpha.T) + I_{Lmin} \quad (2)$$

An expression for ripples I_L (t) is extracted from the equation (3)

$$\Delta I_L = I_{Lmax} - I_{Lmin} = \frac{V_{in}}{V_{out}}.(\alpha.T) \quad (3)$$

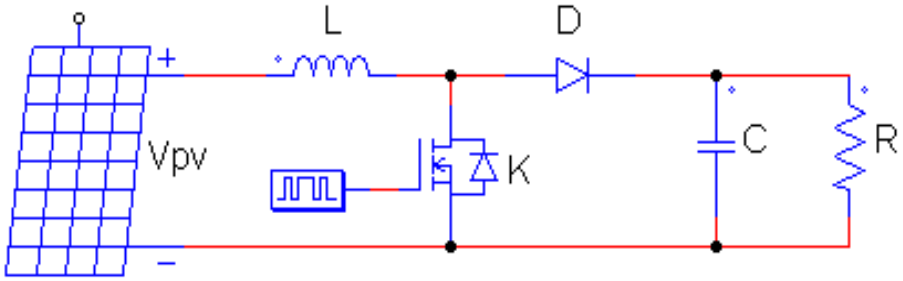

Fig. 2. Solar PV integrated with DC–DC boost converter

b) Dimensioning of the spiral inductor

The dimensions of the inductor to be integrated in the boost converter will be determined by the characteristics indicated in table 2.

Table 2. Converter specifications

Characteristics	Symbol	Value
Input voltage	Vin	3 [V]
Output voltage	Vout	5 [V]
Output power	Pout	3,6 [W]
Operating frequency	f	100 MHz

The calculated value of inductance is given by the equation (4):

$$L = \frac{V_{in} \cdot D}{f \cdot \Delta I_L} \quad (4)$$

Where:
L: Inductance [H]
Vin : Minimum input voltage [V]
D : Duty cycle
f : Switch frequency [Hz]
ΔI_L: Inductor current ripple [A]

The maximum duty cycle for the boost converter is given by the equation (5):

$$D = 1 - \frac{V_{in(min)}}{V_{out}} = 1 - \frac{3}{5} = 0,4 \quad (5)$$

Since the inductor current ripple is unknown, it must be calculated using the equation (6):

$$\Delta I_L = 0,4 \cdot I_{out} \cdot \frac{V_{out}}{V_{in}} = 0,4 \cdot 0,72 \cdot \frac{5}{3} = 0,48 \tag{6}$$

To calculate the value of inductance we use equations (5) and (6), in equation (4):

$$L = \frac{3 \cdot 0,4}{100 \cdot 10^6 \cdot 0,48} = 0,025 \ .10^{-6} \left[H \right]$$

A bigger diameter wire should be used for the coil, in order to reduce inductance DC conduction losses. Also, a lesser switching frequency should be selected, to decrease substrate losses. Both of these outcomes will create a physically bigger inductor that may be more expensive but will attain superior efficiency [12, 13]. One more consideration is the form of the inductor. Figure 3, shows the geometric parameters of a planar spiral inductor. These parameters are: width of the conductor (w), spacing between conductor (s), number of turns (n), thickness of the conductor (t), Inner diameter (din) and outer diameter (dout).

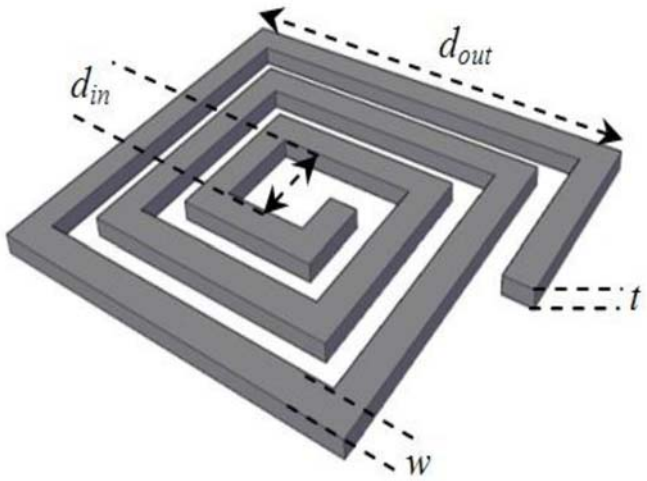

Fig. 3. Schematic of square spiral inductor [14]

The magnetic energy stored is given by equation (7):

$$W = \frac{1}{2}.L.I_{out}^2 = 0,5.\left(0,025 \ .10^{-6}\right).\left(0,72\right)^2 = 6,48.10^{-9} \left[J \right] \tag{7}$$

The volume of the magnetic material (NiFe) is calculated by equation (8):

$$V = \frac{2_{\cdot 0 \cdot r \cdot} W}{B_{max}^2} = \frac{2.\left(4\right).\left(3,14\right).10^{-7}.\left(800\right).\left(6,48.10^{-9}\right)}{\left(0,6\right)^2} = 0,036172\, mm^3 \tag{8}$$

Where, relative permittivity of (NiFe): $\mu_r = 800$, saturation induction Bmax = 0.6 T

In order to calculate the area (A), we set the outer diameter (dout) of the inductor with a length of 2400 [μm] and inner diameter (din) equal 1200 [μm].

Since the inductor is square in shape, we extract from equation (9), the following:

$$\mathrm{A} = \left(\mathrm{d_{out}}\right)^2 = 5,76\, mm^2 \tag{9}$$

To calculate the number of turns for inductor we use Wheeler equation (10):

$$L = \frac{\mu_0 . k_1 . n^2 . d_{avg}}{1 + r . k_2} \tag{10}$$

For a square inductor winding, the coefficients K1 and K2 are as follows 2.34 and 2.75.

The next ties define the form factor and the mean diameter by the following two equations (11) and (12), [15]:

$$r = \frac{d_{out} - d_{in}}{d_{out} + d_{in}} \tag{11}$$

$$d_{avg} = \frac{d_{out} + d_{in}}{2} \tag{12}$$

Equation (13), is extracted from equation (10), (11) and (12):

$$n^2 = \frac{L.\left(1 + k_2.\left(\frac{d_{out} - d_{in}}{d_{out} + d_{in}}\right)\right)}{\mu_0 . k_1 . \left(\frac{d_{out} + d_{in}}{2}\right)} = \frac{0,025.10^{-6}.\left(1 + 2,75.\left(\frac{1200.10^{-6}}{3600.10^{-6}}\right)\right)}{4.(3,14).10^{-7}.(2,34).\left(\frac{3600.10^{-6}}{2}\right)} = 9 \tag{13}$$

It depends to extract the width and thickness of the conductor on the following condition: (w≤2δ) or (t≤2δ)

Where, δ is the skin thickness and obtained by equation (14), [16].

$$\delta = \sqrt{\frac{\rho_{Cu}}{\pi . \mu . f}} = \sqrt{\frac{1,7.10^{-8}}{3,14\left(4.(3,14).10^{-7}\right).100.10^{6}}} = 6,565.10^{-6}\left[m\right] \tag{14}$$

where ρ represent the resistivity of the conductor, ρ_{Copper} = 1.7·10 $^{-8}$ [Ωm] and μ its magnetic permeability. By fulfilling the condition t≤2δ, t is obtained as follows t=13 [µm]

The width of conductor w is derived from the equations (15):

$$S = w.t \tag{15}$$

Where, S represent the conductor section and is equal to 1755 [mm^2]. By applying the calculation to equation (15), we get the value of the width of conductor, which is equal to w=135 [µm]

The spacing between conductors is expressed by the equation (16):

$$s = \frac{d_{out} - d_{in} - 2wn}{2(n-1)} = \frac{2400.10^{-6} - 1200.10^{-6} - 2.\left(135.10^{-6}\right).3}{2(3-1)} = 97,5\left[\mu m\right] \tag{16}$$

The length of the trace is expressed by the equation (17):

$$l = 4n\left[d_{out} - (n-1)s - nw\right] - s = 21,5\left[mm\right] \tag{17}$$

After calculations, we obtain the values of the dimensions of the spiral inductor, summarized in the following table 3:

Table 3. The geometric parameters of the inductor

Geometrical parameters	Symbol	Dimensioning results
Outer Diameter	*dout*	2,4 mm
Inner Diameter	*din*	1,2 mm
Number of turns	*n*	3
Thickness of the conductor	*t*	13 µm
Width of the conductor	*w*	135 µm
Spacing between conductor	*s*	97,5 µm
Length of the conductor	*l*	21,5 mm

We have considered the equivalent circuit shown in figure 4.

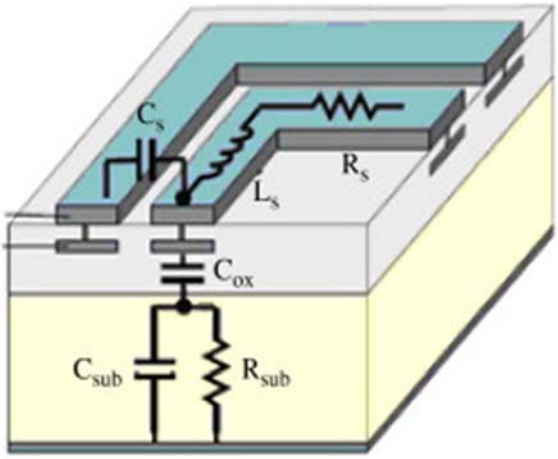

(a)

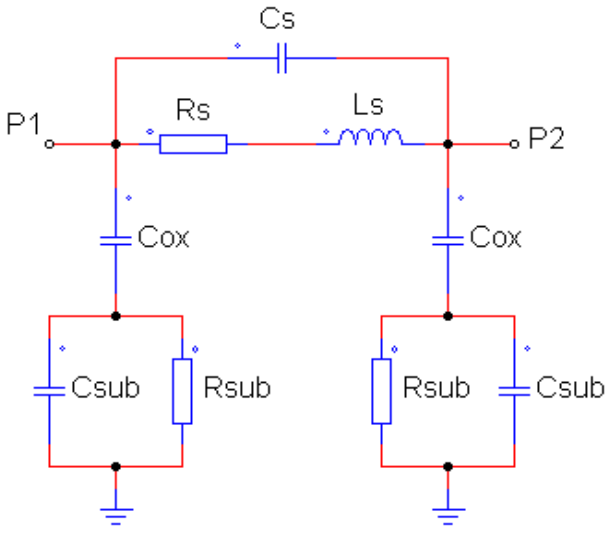

(b)

Fig.4. (a) Transverse section of a spiral inductor, (b) Electrical circuit equivalent in π of a spiral inductor [17]

This electrical parameters of spiral inductor are calculated using the formulas [18, 19], found in table 4, which will serve as the mainstay for the optimization and simulation.

Table 4. Formulas for electrical parameters

Electric parameters	Analytical equation	Value
Series resistance	$R_s = \frac{\rho_{Cu}.l}{w.\delta\left(1-e^{\left(-\frac{t}{\delta}\right)}\right)}$	0,478 [Ω]
Coupling capacitance	$C_s = \frac{w^2.n.\varepsilon_{ox}}{t_{ox}}$	0,0629 [pF]
Oxide capacitance	$C_{ox} = \frac{w.l.\varepsilon_{ox}}{2.t_{ox}}$	1,669 [pF]
Substrate resistance	$R_{sub} = \frac{2.h_{sub}.\rho_{sub}}{l.w}$	0,537 [kΩ]
Substrate capacitance	$C_{sub} = \frac{l.w.\varepsilon_{sub}}{2.h_{sub}}$	3,031 [pF]

where, t_{ox} is the oxide thickness between the spiral and the substrate (t_{ox}=30 µm), ρ_{cu} is the resistivity of the metal (ρ_{cu}=1,7 . 10^{-8} Ωm), ε_{ox} is the oxide permittivity (ε_{ox}=3,9) (ε_0=8,85 pF.m^{-1}), h_{sub} is the substrate height (h_{sub}=50 µm), ρ_{sub} is the substrate resistivity (ρ_{sub}= 18,5 Ωm), ε_{sub} is the substrate permittivity (ε_{sub}=11,8), (δ) is the skin depth and finally (μ) is the magnetic permeability of free space.

SIMULATION OF MAGNETIC BEHAVIOR

To get closer to reality and based on the results of the dimensioning as shown in table 2, we will show the geometry of our spiral inductor model designed in 3D as shown in figure 5.

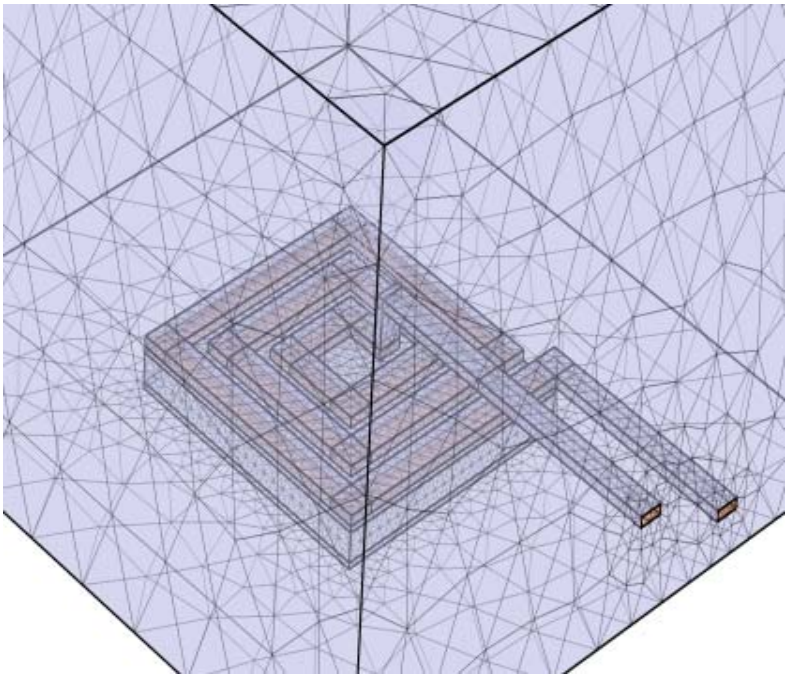

Fig. 5. Structure of the spiral inductor simulated with the mesh of the field of study

a) Distribution of electric potential and magnetic flux density

Figure 6, shows the distribution of the current density and magnetic flux density in the square planar coil in 3D.

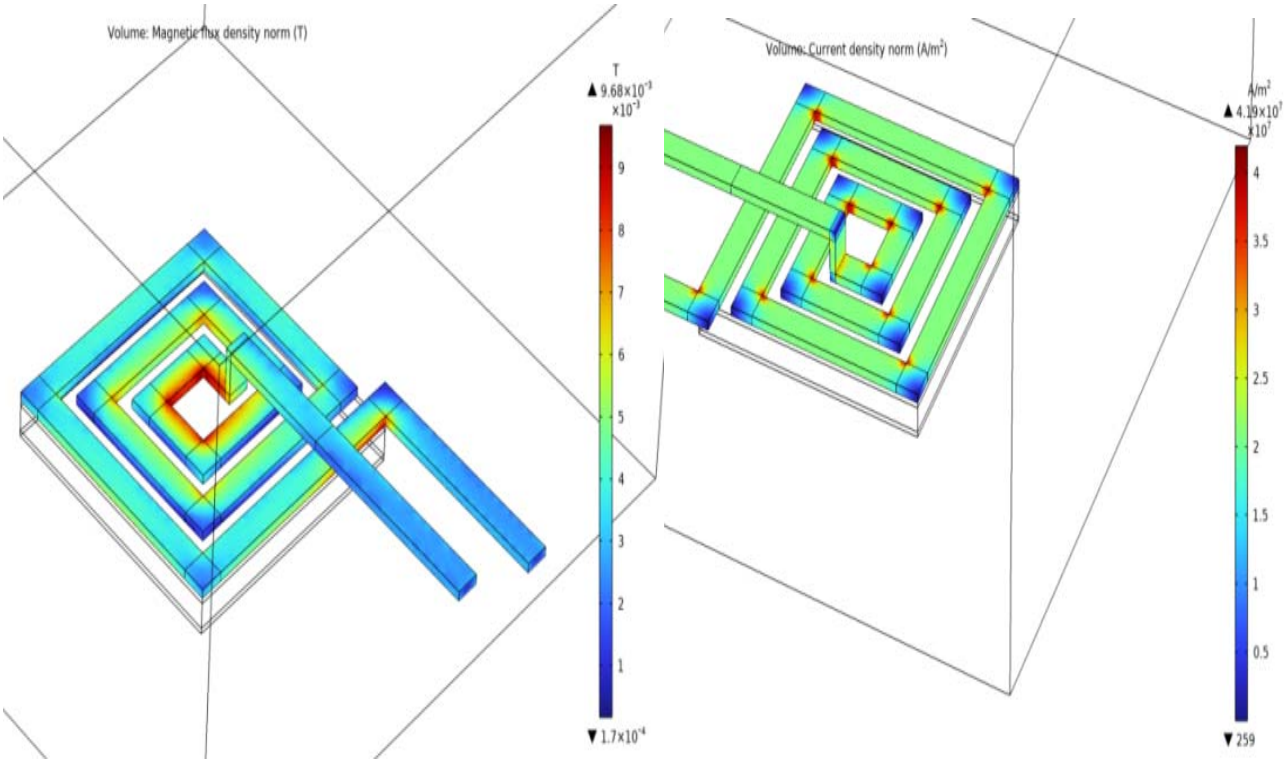

(a) (b)

Fig. 6. (a) 3D view for the magnetic flux density, (b) 3D view shows the current density

b) Selection of the optimal frequency

To keep the conductor size within the appropriate range, the optimum frequency *f* should be chosen to limit overheating due to skin effect or lack of energy due to large losses. As such, the simulations was carried to observe the magnetic flux and the current density of three different frequencies: [1 kHz, 2223 kHz and 5001 kHz]. The simulation results are shown in figure 7. It's noticeable a considerable augment in magnetic flux density for more frequency; this is correlated to the density of electric current in the conductor, which is more important in added frequency (figure 8).

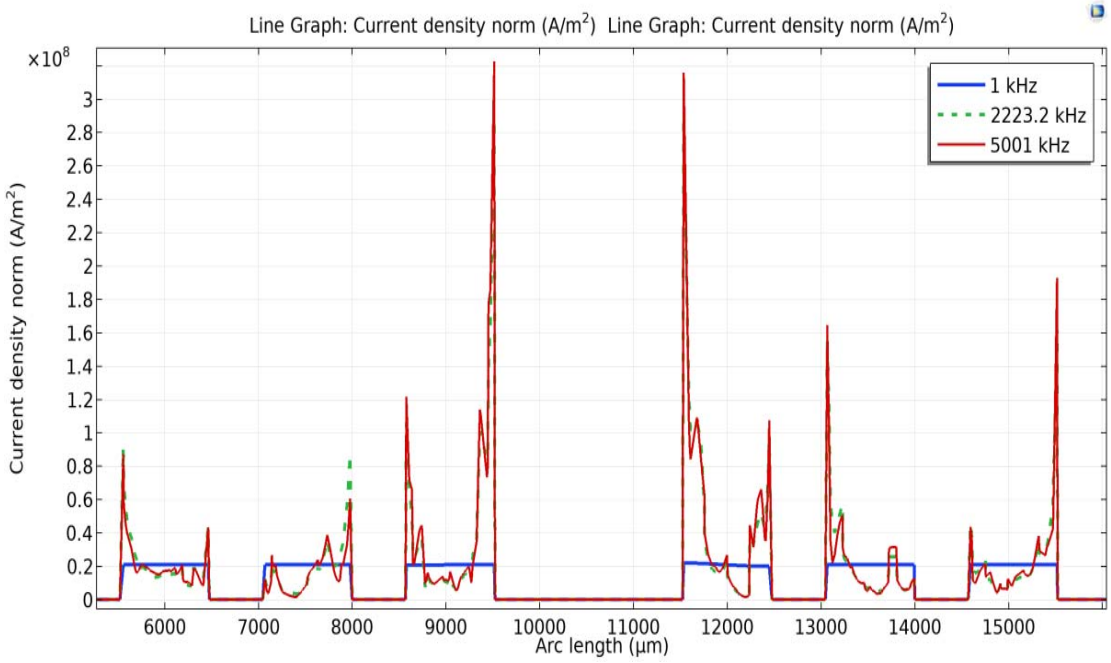

Fig. 7. Simulations of the current density norm according to the arc length mentioned in spiral inductor

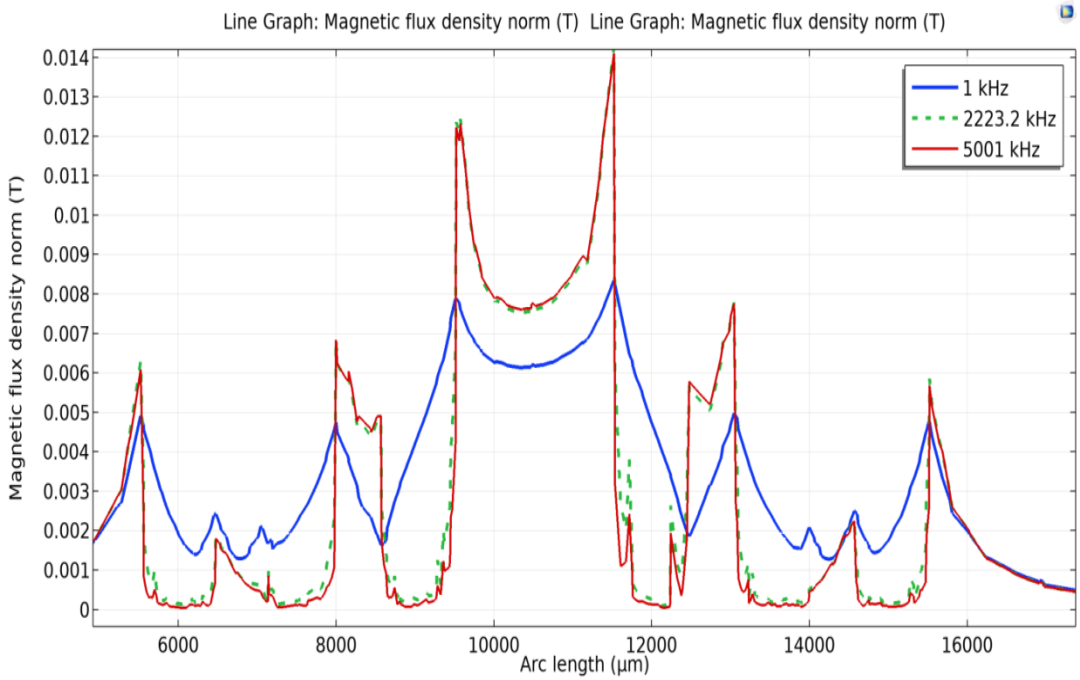

Fig. 8. Cross-sectional plot magnetic flux density along the arc length mentioned in spiral inductor

c) Simulation of the electric model of the photovoltaic system

Figure 9, shows the simulation circuit of a photovoltaic system with a boost converter containing the electrical circuit of integrated spiral inductor model (figure 4):

Figure 10, shows the current flowing in the inductor and the voltage and current produced by the boost converter. The obtained simulation results show us that the output voltage Vout and the output current Iout are continuous, The obtained values are fairly close to the specification of the boost converter DC-DC. These results show that the spiral inductor integrated into the boost converter works well. Thus, we can ensure that the geometric dimensions of the integrated spiral inductor and its electrical parameters are well defined.

Figure 10(a), shows the simulated output current (*Iout*) at a switching frequency of 100 MHz. It is noted that the output current is constant starting from the first 40 [ms]. The boost converter delivers an output current of about 0,72 [A]. In addition, a similar observation is observed for the output voltage (*Vout*) as shown in figure 10(b), where the mode is transient in the first 20ms. Also, we notice that the output voltage increased from 3[V] to 5[V]. The waveform current across the inductor terminals shown in figure 10(c), never crosses the zero value, where this change ranges between 0,4829 [A] and 0,4871[A]. Therefore, the continuous conduction mode is respected.

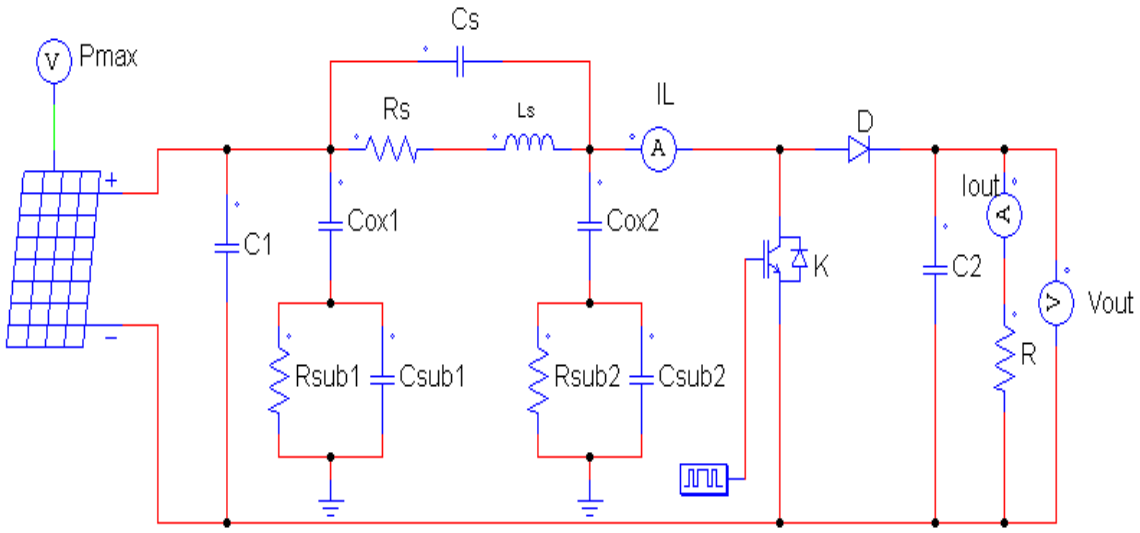

Fig.9. Photovoltaic system and boost converter with an integrated spiral inductor

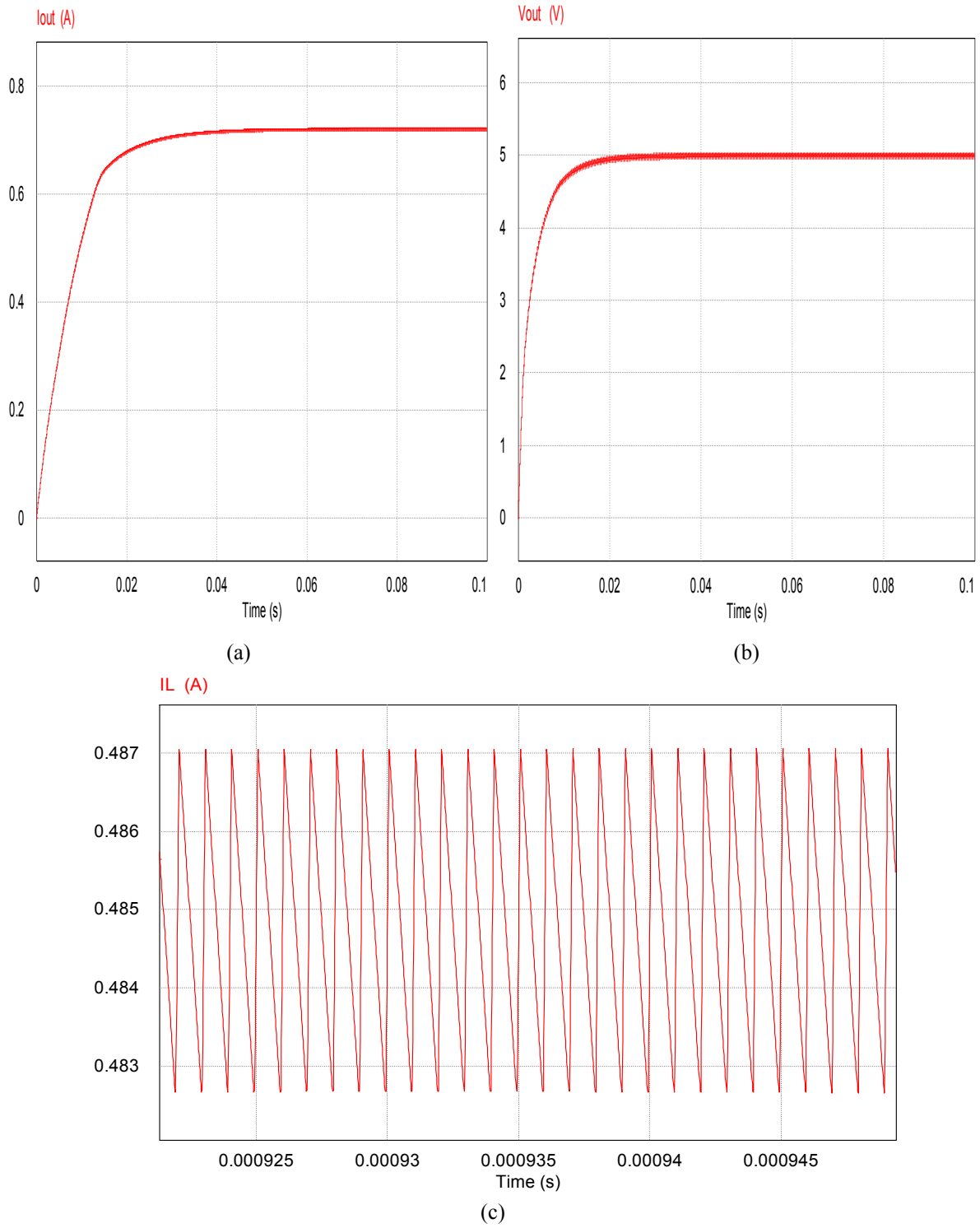

Fig. 10. Waveforms in boost converter, (a) Output current, (b) Output voltage, (c) Current flowing in the spiral inductor

CONCLUSION

In this article, we have presented the design and simulation integrated spiral coil a boost converter. First, we have calculated the geometrical and electrical parameters of planar inductor. Next, by using the software COMSOL 3.5a, we have visualized the distribution of the lines of field of our spiral inductor in order to know if they do not overflow and thus do not disturb the other elements of the boost converters. We also visualized the density of the magnetic flux and the electric potential. Finally, by using a software simulation PSIM 9.0, we have extracted the waveforms of the output voltages and output current in boost converter. We conclude that the results of dimensioning in this paper are interesting indeed.

REFERENCES

[1] P. Khazaei, *et al*, "A High Efficiency DC/DC Boost Converter for Photovoltaic Applications," International Journal of Soft Computing and Engineering (IJSCE), vol. 6, n.2, p 31-37, 2016. Disponible en: https://www.ijsce.org/portfolio-item/B2838056216/

[2] A. Mamizadeh, B. A. Mustafa, N. Genc, "Planar Flyback Transformer Design for PV Powered LED Illumination," International Journal of Renewable Energy Research (IJRER), vol. 11, n.1, p 439-445, 2021. Disponible en: https://www.ijrer.org/ijrer/index.php/ijrer/article/view/11695/pdf

[3] M. R. Benzidane, *et al*, "Miniaturization and Optimization of a DC–DC Boost Converter for Photovoltaic Application by Designing an Integrated Dual-Layer Inductor Model," Transactions on Electrical and Electronic Materials, vol. 23, p 462–475, 2022. Disponible en: https://link.springer.com/article/10.1007/s42341-021-00370-9

[4] K.T. Ahmed, M. Datta, N. Mohammad, " A novel two switch non-inverting buck–boost converter-based maximum power point tracking system, " International Journal of Electrical and Computer Engineering (IJECE), vol. 3, n.4, p 467–477, 2013. Disponible en: https://ijece.iaescore.com/index.php/IJECE/article/view/5436/4965

[5] D. Guendouz, A. Laidi, "Dimensioning of a non-planar wound inductor of a Buck converter," PRZEGLĄD ELEKTROTECHNICZNY, vol. 20, n.12, p 81-84, 2020. Disponible en: http://pe.org.pl/articles/2020/12/15.pdf

[6] Q. Zhao and F. Lee, "High-Efficiency, High Step-Up DC-DC Converters," IEEE Transactions on Power Electronics, vol.18, n.1, p 65-73, 2003. Disponible en: http://profs.hut.ac.ir/~naghizadeh/PE1%2093-2%20Term%20Papers/920626770.pdf

[7] A. Namoune, R. Taleb, N. Mansour, "Design and modeling of solenoid inductor integrated with FeNiCo in high frequency," TELKOMNIKA (Telecommunication Computing Electronics and Control), vol.18, n. 4, p 1746-1753, 2020. Disponible en: http://telkomnika.uad.ac.id/index.php/TELKOMNIKA/article/view/12139/8404

[8] K. V. G. Raghavendra, *et al*, "A Comprehensive Review of DC–DC Converter Topologies and Modulation Strategies with Recent Advances in Solar Photovoltaic Systems," electronics, vol. 31, n. 9, p 1- 41, 2020. Disponible en: https://www.mdpi.com/2079-9292/9/1/31

[9] R. Gladwin Antony, *et al*, " Design of Solar Charging Case for Mobile Phones," Journal of Physics: Conference Series (International Conference on Physics and Energy), vol. 2040, 2021. Disponible en: https://iopscience.iop.org/article/10.1088/1742-6596/2040/1/012031/pdf

[10] R. Ayop, C. W. Tan, "Design of boost converter based on maximum power point resistance for photovoltaic applications," Solar energy, vol.160, n.15, p 322-335, 2018. Disponible en: https://doi.org/10.1016/j.solener.2017.12.016

[11] A. Pradhan, B. Panda, "A simplified design and modeling of boost converter for photovoltaic sytem," International journal electrical and computer engineering, vol.8, n.1, p 141-149, 2018. Disponible en: https://ijece.iaescore.com/index.php/IJECE/article/view/10108/8100

[12] H. Hernandez, W. Noije. "Fully integrated boost converter for thermoelectric energy harvesting in 180 nm CMOS," Analog integrated circuits and signal processing, vol. 82, n.1, P 17–23, 2015. Disponible en: https://www.academia.edu/79998140/Fully_integrated_boost_converter_for_thermoelectric_energy_harvesting

[13] A. Namoune, *et al*, "Integrated square shape inductor with magnetic core in a buck converter DC-DC," Przeglad Elektrotechniczny, vol. 95, n.9, p 57-61, 2019. Disponible en: http://pe.org.pl/articles/2019/9/11.pdf

[14] S. Saravanan, N.R. Babu, "A modified high step-up non-isolated DC–DC converter for PV application, " Journal of Applied Research and Technology, vol. 15, n.3, p 242–247, 2017. Disponible en: https://jart.icat.unam.mx/index.php/jart/article/view/655

[15] A. Namoune, *et al*, "Design and modeling of integrated octagonal shape inductor with substrate silicon in a buck converter," Indonesian journal of electrical engineering and informatics (IJEEI), vol. 7, n. 3, p 527-534, 2019. Disponible en: http://section.iaesonline.com/index.php/IJEEI/article/view/942

[16] A. Ammouri, T. Ben-Salah, H. Morel, "A spiral planar inductor: An experimentally verified physically based model for frequency and time domains," International journal of numerical modelling, vol.31, n.1, p 1–13, 2018. Disponible en: https://onlinelibrary.wiley.com/doi/abs/10.1002/jnm.2272

[17] M. H. Bechir, *et al*, "Planar inductor equivalent circuit model taking into account magnetic permeability, loss tangent, skin and proximity effects versus frequency,"Analog integrated circuits and signal processing, vol.88, n.1, p 105–113, 2016. Disponible en: https://link-springer-com.sndl1.arn.dz/content/pdf/10.1007/s10470-016-0697-1.pdf

[18] S.E. Babaa, "Novel Switch Adaptive Control to Improve the Efficiency of Boost Converter in Photovoltaic Systems," Journal of power and energy engineering, vol.5, n. 7, p 1-14, 2017. Disponible en: https://www.scirp.org/journal/paperinformation.aspx?paperid=77470
[19] A. Namoune, R. Taleb, N. Mansour, "Simulation of an integrated spiral inductor and inter-digital capacitor in a buckmicro converter," AUTOMATIKA, vol.63, n.4, p 1-9, 2022. Disponible en: https://www.tandfonline.com/doi/epdf/10.1080/00051144.2022.2142572?needAccess=true&role=button

CONFLICT OF INTERESTS

The authors declare that there are no conflicts of interest.

AUTHORS 'CONTRIBUTION

Abdelhadi Namoune: https://orcid.org/0000-0001-9017-065X
Research design. Mathematical modeling and simulation of the models. He participated in the analysis of the results, writing the draft of the article, the critical review of its content, and in the final approval.

Rachid Taleb: https://orcid.org/0000-0002-9874-0423
Research design. Mathematical modeling and simulation of the models. He participated in the analysis of the results, writing the draft of the article, the critical review of its content, and in the final approval.

Mohammed Ridha Benzidane: https://orcid.org/0000-0003-1761-4618
Research design. Mathematical modeling and simulation of the models. He participated in the analysis of the results, writing the draft of the article, the critical review of its content, and in the final approval.